JOURNAL OF GEOPHYSICAL RESEARCH: ATMOSPHERES, VOL. 118, 917–933, doi:10.1029/2012JD018196, 2013

Improving the temporal and spatial distribution of CO_2 emissions from global fossil fuel emission data sets

Ray Nassar,[1] Louis Napier-Linton,[1,2] Kevin R. Gurney,[3] Robert J. Andres,[4] Tomohiro Oda,[5,6] Felix R. Vogel,[1] and Feng Deng[7]

Received 30 May 2012; revised 29 October 2012; accepted 21 November 2012; published 18 January 2013.

[1] Through an analysis of multiple global fossil fuel CO_2 emission data sets, Vulcan emission data for the United States, Canada's National Inventory Report, and NO_2 variability based on satellite observations, we derive scale factors that can be applied to global emission data sets to represent weekly and diurnal CO_2 emission variability. This is important for inverse modeling and data assimilation of CO_2, which use in situ or satellite measurements subject to variability on these time scales. Model simulations applying the weekly and diurnal scaling show that, although the impacts are minor far away from sources, surface atmospheric CO_2 is perturbed by up to 1.5−8 ppm and column-averaged CO_2 is perturbed by 0.1−0.5 ppm over some major cities, suggesting the magnitude of model biases for urban areas when these modes of temporal variability are not represented. In addition, we also derive scale factors to account for the large per capita differences in CO_2 emissions between Canadian provinces that arise from differences in per capita energy use and the proportion of energy generated by methods that do not emit CO_2, which are not accounted for in population-based global emission data sets. The resulting products of these analyses are global $0.25° \times 0.25°$ gridded scale factor maps that can be applied to global fossil fuel CO_2 emission data sets to represent weekly and diurnal variability and $1° \times 1°$ scale factor maps to redistribute spatially emissions from two common global data sets to account for differences in per capita emissions within Canada.

Citation: Nassar, R., L. Napier-Linton, K. R. Gurney, R. J. Andres, T. Oda, F. R. Vogel, and F. Deng (2013), Improving the temporal and spatial distribution of CO_2 emissions from global fossil fuel emission data sets, *J. Geophys. Res. Atmos.*, *118*, 917–933, doi:10.1029/2012JD018196.

1. Introduction

[2] There is increasing interest in the estimation of CO_2 sources and sinks by inverse modeling or data assimilation techniques; however, current approaches typically do not optimize estimates of CO_2 emissions from fossil fuel combustion [*Gurney et al.*, 2002, 2004; *Baker et al.*, 2006; *Peters et al.*, 2005, 2007; *Nassar et al.*, 2011; *Takagi et al.*, 2011]. Instead, fossil fuel emissions of CO_2 are usually treated as a known quantity in the inversion (i.e., with zero uncertainty), so that CO_2 fluxes from the terrestrial biosphere and oceans, which are considered more uncertain, can be optimized using measurements of atmospheric CO_2. As a result of this approach, errors in the fossil fuel emissions are hidden and instead cause systematic errors in the biospheric and oceanic CO_2 flux estimates. As more advanced data assimilation systems are developed with the aim of producing CO_2 flux estimates with lower (and better characterized) uncertainties to improve our understanding of carbon cycle science or to inform policy discussions, parallel efforts are required to improve all components of the assimilation system.

[3] Global fossil fuel CO_2 emission data sets are typically developed by spatially distributing emissions from national CO_2 emission totals reported under the United Nations Framework Convention on Climate Change (UNFCCC) or other global compilations [e.g., *Andres et al.*, 2012]. The magnitude of the uncertainty in the national totals is thought to be less than ~8% for the developed countries (Annex B countries under the Kyoto Protocol to the UNFCCC), which have strict emissions accounting systems [*Andres et al.*, 1996]. Uncertainties are greater for the developing countries (non-Annex B countries) [*Guan et al.*, 2012], which

[1]Climate Research Division, Environment Canada, Toronto, Ontario, Canada.
[2]Department of Physics, University of Waterloo, Waterloo, Ontario, Canada.
[3]School of Life Sciences, Arizona State University, Tempe, Arizona, USA.
[4]Oak Ridge National Laboratory, Oak Ridge, Tennessee, USA.
[5]Colorado State University, Fort Collins, Colorado, USA.
[6]Global Monitoring Division, National Oceanic and Atmospheric Administration, Earth System Research Laboratory, Boulder, Colorado, USA.
[7]Department of Physics, University of Toronto, Toronto, Ontario, Canada.

Corresponding author: R. Nassar, Climate Research Division, Environment Canada, 4905 Dufferin Street, Toronto, Ontario M3H 5T4, Canada. (ray.nassar@ec.gc.ca)

2169-897X/13/2012JD018196

continue to make an increasing contribution to global CO_2 emissions, now exceeding the emissions from developed countries [*Peters et al.*, 2011]. Errors related to the spatial and temporal distribution in emission data sets are more difficult to quantify but can be proportionally much larger than the national totals. Although these emission data sets typically include interannual variability, which has a major impact on the estimation of annual CO_2 fluxes, the implementation of intra-annual temporal variability is still novel. The gridded $1° \times 1°$ emission data set from the Carbon Dioxide Information and Analysis Center (CDIAC) [*Andres et al.*, 2011], which distributes national emissions according to population density, includes global seasonal variability using monthly emission totals for many countries. The Open-Source Data Inventory of Anthropogenic CO_2 Emission (ODIAC) distributes national emissions based on satellite observations of nighttime lights and information on 17,688 power plants [*Oda and Maksyutov*, 2011] providing emissions at a selection of spatial resolutions ($1° \times 1°$, $0.05° \times 0.05°$, or $0.01° \times 0.01°$). A new version of ODIAC (v3.0) includes a seasonal cycle using the CDIAC approach [*Maksyutov et al.*, 2012]. The Emission Database for Global Atmospheric Research (EDGAR; http://edgar.jrc.ec.europa.eu/index.php) version 4.2 distributes national emission totals using a geographic database with data such as the locations of energy and manufacturing facilities, road networks, shipping routes, human and animal population density, and agricultural land use, resulting in $0.1° \times 0.1°$ annual emission maps, but EDGAR v4.2 has no intra-annual variability. On the other hand, the Vulcan fossil fuel emission data product [*Gurney et al.*, 2009], derived from a complex mix of data from power plant CO emissions, transportation statistics, and a variety of socioeconomic indicators, gives hourly CO_2 emissions at high spatial resolution ($10 \times 10\,km^2$ and $0.1° \times 0.1°$) but is limited to the United States for the year 2002. Another regional high-spatial- and high-temporal-resolution data set also exists but includes only U.S. power plants [*Pétron et al.*, 2008].

[4] The absence of temporal variability on the scale of days or weeks in CDIAC and ODIAC, or any intra-annual variability in standard EDGAR emission data, means that nearly all models using them assume constant emissions for those time scales, even though energy use is known to exhibit weekly and diurnal cycles. A set of weekly and diurnal temporal curves was provided as an EDGAR v3.2 provisional data product determined using emissions patterns from Western Europe, as an exploratory method of addressing this problem (http://themasites.pbl.nl/en/themasites/edgar/documentation/content/Temporal-variation.html). Although the associated disclaimer warns of high uncertainty in applying the temporal curves to other parts of the world, they have been applied to the global $1° \times 1°$ EDGAR v3.2 emission data set with few modifications as part of the CO_2 Release and Oxygen Uptake from Fossil Fuel Emission Estimate (COFFEE) [*Steinbach et al.*, 2011]. The Institute of Energy Economics and the Rational Use of Energy (IER) at the University of Stuttgart is also actively working in the area of short-time-scale variability in CO_2 emissions from fossil fuels for Europe [*Pregger et al.*, 2007; see also *IER Emission Data*, 2008 (http://carboeurope.ier.uni-stuttgart.de/)].

[5] The importance of seasonal variability in fossil fuel emissions to CO_2 inverse modeling has been demonstrated in previous work [*Gurney et al.*, 2005; *Erickson et al.*, 2008; *Peylin et al.*, 2011]. The importance of weekly or diurnal variability in CO_2 inverse modeling has received less attention, but, in a multimodel experiment using IER hourly emission data and EDGAR FT2000 data with hourly variability, *Peylin et al.* [2011] explore the impact of intra-annual variability on CO_2 simulations over Europe. Although *Peylin et al.* [2011] determined that the impact of the intra-annual variability in emissions is less than the impact of using different transport fields, it was still found to be an important factor, and the authors referred to an urgent need for more work on improving the spatial and temporal distributions of fossil fuel emission data. One important reason for including weekly or diurnal variability is the fact that the measurements used in inverse modeling studies are subject to these temporal scales. CO_2 flask samples are commonly collected only once or twice per week and correspond to a specific time of the day (usually afternoon) [*Conway et al.*, 1994]. The use of continuous in situ CO_2 measurements (which span the diurnal and weekly cycles) is also becoming more common [*Worthy et al.*, 2003]. With the arrival of novel satellite observations of CO_2 from missions such as the Greenhouse Gases Observing Satellite (GOSAT) [*Yokota et al.*, 2009; *Yoshida et al.*, 2011] and the upcoming Orbiting Carbon Observatory 2 (OCO-2) mission [*Crisp et al.*, 2004, 2012], new, advanced data assimilation systems are being developed to take advantage of these data. As additional CO_2 satellites enter into operation and the data assimilation systems mature further, they may eventually be used for international treaty monitoring and verification purposes [*Pacala et al.*, 2010]. Polar-orbiting nadir-viewing satellites (such as GOSAT and OCO-2) usually have sun-synchronous orbits, which have a fixed equator-crossing time and thus provide observations at a set local time of the day. Satellite observations of NO_2 from such orbits have already demonstrated clear variability in anthropogenic emissions over the course of a week or the diurnal cycle [*Beirle et al.*, 2003; *Boersma et al.*, 2009]. Because CO_2 has a longer atmospheric lifetime than NO_2, short-time scale variability will have less of an impact on CO_2 because enhancements relative to background levels are smaller, but accounting for this variability in advanced CO_2 data assimilation systems (aimed at making more accurate estimates) could reduce errors in the optimization of CO_2 fluxes from other sources and sinks.

[6] In this work, we have developed a set of seven scale factor maps for each day of the week (weekly) and 24 scale factor maps for each hour of the day (diurnal) at 0.25° 0.25° resolution globally. We refer to this new data product as Temporal Improvements for Modeling Emissions by Scaling (TIMES). The TIMES weekly- and diurnal-scale factor maps can be applied to global CO_2 emission data sets lacking these modes of temporal variability, such as CDIAC, ODIAC, EDGAR, and others, to reduce errors in 3D CO_2 modeling or data assimilation. This study was motivated by the need to provide accurate fossil fuel emissions for an advanced global CO_2 data assimilation system now under development at Environment Canada, which will use both in situ and satellite observations of CO_2, will apply data assimilation methods from numerical weather prediction, and

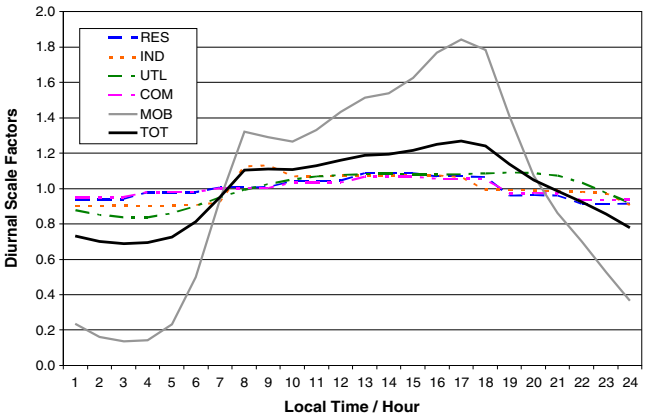

Figure 1. Dimensionless hourly scale factors for the five sectors with diurnal variability (RES, residential; IND, industrial; UTL, electric utilities; COM, commercial; MOB, on-road mobile) in the Vulcan emission data product, along with the weighted total (TOT; which also includes the remaining emissions) for the contiguous United States in 2002. These were calculated by averaging the temporal profiles from the four time zones of the contiguous United States with the necessary offset. MOB has the largest diurnal amplitude of all sectors, whereas RES and COM are almost indistinguishable, with small diurnal amplitudes.

will attempt to account for all sources of uncertainty. This system is still being developed, so we test the sensitivity of surface atmospheric CO_2 distributions to these temporal-scale factors with the GEOS-Chem model [*Nassar et al.*, 2010]. In the process of developing the temporal-scale factors, limitations in current methods of spatially distributing emissions were also highlighted. One key limitation relates to the wide range of variability in per capita emissions that can exist within a country, which is not accounted for explicitly in population-based inventories; therefore, as an additional data product, a separate set of $1° \times 1°$ Canadian scale factor maps was developed that could be applied to the CDIAC and ODIAC emission inventories to improve the spatial distribution of Canadian CO_2 emissions.

2. Methods

2.1. Diurnal Variability

[7] Our approach to developing the TIMES scale factor maps begins with an analysis of the Vulcan emission data product v2.0, which provides CO_2 emissions for the contiguous United States in 2002 at $10 \times 10\,km^2$ and $0.1° \times 0.1°$ resolution. (The v2.2 update also includes Alaska at $10 \times 10\,km^2$.) Vulcan emissions are divided into eight sectors: residential, commercial, industrial, electricity production, mobile on-road, mobile nonroad, cement manufacture, and aircraft [*Gurney et al.*, 2009]. The residential, commercial, industrial, electricity production, and mobile on-road sectors exhibit diurnal variability, whereas the other sectors are temporally constant in Vulcan at the diurnal scale (although they have monthly time structure).

[8] Diurnal variability in anthropogenic CO_2 emissions is related to both geophysical cycles (i.e., heating/cooling needs of a building changing with diurnal cycle in outdoor temperatures) and sociodemographic patterns, such as the time of day when people drive to/from work. Representing the geophysical contribution to the diurnal cycle could perhaps be accomplished best by relating emissions to the local solar time (which varies continuously as a function of longitude); however, representing the sociodemographic aspect of diurnal variability would suggest the use of standard international time zones, which are essentially a stepwise representation of solar time. Therefore, we determined the diurnal cycle for emissions from each Vulcan sector separately for the four time zones in the contiguous United States. Averaging the results from the different time zones and accounting for their hourly offsets (neglecting daylight saving time) gives the United States diurnal profiles for these sectors shown in Figure 1, where a value of 1 represents the daily mean for each sector. The profile for total emissions shown in Figure 1 is dependent on the fraction that each sector contributes to the total (sector weighting).

[9] Based on Vulcan for the United States (at $0.1° \times 0.1°$) and EDGAR v4.2 for other countries, the proportion of the emissions from the residential, industrial, electricity production, mobile on-road, and "other" sectors was determined for the 20 highest CO_2-emitting countries in 2008 (Table 1), which account for 80% of global CO_2 emissions from fossil fuel combustion and cement manufacture [*Andres et al.*, 2011]. The diurnal profiles for each sector from Vulcan were each associated with a sector from EDGAR, then weighted according to the EDGAR sector proportions to determine a diurnal profile of total CO_2 emissions for the other 19 high-emitting countries. The remaining countries of the world were each associated with a proxy country from the top 20 CO_2-emitting countries to approximate their diurnal variability. Figure 2 shows these proxy country groups; for example, the diurnal variability of Portugal was based on

Table 1. Fraction of Emissions per Source Sector for the 20 Highest-Emitting Countries in 2008 From EDGAR v4.2 and for the Contiguous United States in 2002 From Vulcan[a]

Country	Residential	Industrial	Utilities	Mobile	Other
China	0.067	0.368	0.494	0.046	0.025
United States	0.109	0.142	0.420	0.278	0.050
India	0.108	0.238	0.552	0.081	0.022
Russia	0.116	0.201	0.528	0.116	0.040
Japan	0.129	0.246	0.426	0.163	0.036
Germany	0.198	0.155	0.416	0.178	0.053
Canada	0.158	0.204	0.303	0.241	0.094
Iran	0.346	0.398	0.197	0.025	0.034
United Kingdom	0.183	0.144	0.382	0.221	0.071
South Korea	0.107	0.213	0.493	0.151	0.036
Mexico	0.075	0.244	0.332	0.320	0.029
Italy	0.170	0.213	0.309	0.249	0.058
South Africa	0.077	0.153	0.621	0.130	0.018
Saudi Arabia	0.013	0.230	0.391	0.300	0.066
Indonesia	0.071	0.357	0.363	0.158	0.050
Australia	0.040	0.144	0.608	0.166	0.042
Brazil	0.093	0.380	0.123	0.356	0.049
France	0.226	0.223	0.157	0.306	0.088
Spain	0.097	0.217	0.301	0.299	0.086
Ukraine	0.136	0.313	0.412	0.100	0.039
U.S.-Vulcan	0.066	0.188	0.400	0.258	0.088

[a]The four sectors shown have short-time scale variability in Vulcan and are also present in EDGAR. "Other" is the sum of sectors that did not have short-time scale variability in Vulcan. The "Other" value for Vulcan also includes the commercial sector, which does have short-time scale variability but is not defined in EDGAR.

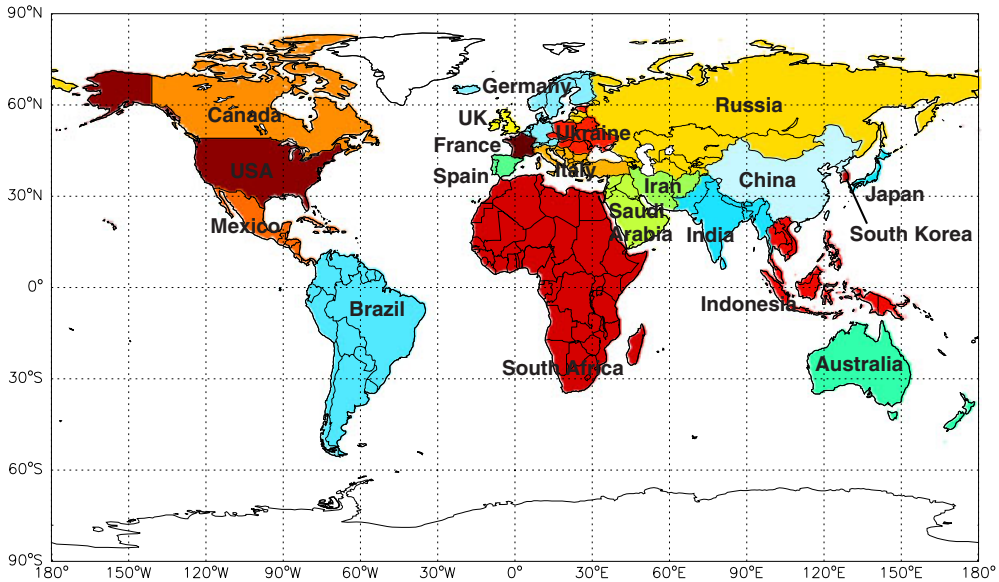

Figure 2. Twenty proxy country groups for weekly and diurnal scale factors, for which each group is associated with one of the 20 highest CO_2-emitting countries (Table 1). The highest-emitting countries were based on the CDIAC ranking for 2008, but these groupings differ from the 21 proxy country groups used by *Andres et al*. [2011].

that of Spain, New Zealand was based on Australia, and all African nations were based on South Africa. The approach of using of the highest-emitting countries as proxies was also applied in the CDIAC emission product to obtain monthly variability [*Andres et al*., 2011]. Although our proxy country groups sometimes differ from those of *Andres et al*. [2011], their work showed that the sensitivity to proxy country selection was low (for the global seasonal cycle), partially because the emissions from nonproxy countries are relatively low. Canadian provincial and territorial energy sector information is readily available in Part 3 of Canada's *National Inventory Report* [*NIR*, 2011], so we treated each Canadian province and territory separately, using these factors (Table 2) instead of the EDGAR values for Canada. Canadian provincial differences and the National Inventory Report are discussed in detail in section 2.3.

[10] An open-source time zone shape file was gridded (using Geographic Information Systems [GIS] software) to produce a $0.25° \times 0.25°$ global time zone map. The 399 time zone shapes were then grouped into 24 time zones, essentially rounding off time zones with offsets of less than 1 h and aggregating time zone shapes with the same standard time but different daylight saving time rules. A dimensionless scale factor from the diurnal profile of total CO_2 emissions for each country was then gridded to $0.25°$ $0.25°$ using country and provincial masks at this resolution to give global scale factors maps for each hour of the day, with appropriate offsets for time zones. Figure 3 shows global diurnal scale factor maps for 00, 06, 12, and 18 Coordinated Universal Time (UTC). These dimensionless factors can be applied to scale emissions from an emission data set without variability in total emissions over a 24 h period. The factors have six or more significant digits to ensure conservation of mass for total emissions after scaling, not to imply that true values are known to this precision.

[11] The sensitivity of surface atmospheric CO_2 to the diurnal scale factors was determined using the GEOS-Chem model's CO_2 simulation mode [*Nassar et al*., 2010]. Version 9.01.01 of the model was run using GEOS-5 meteorology for 2009 at $2° \times 2.5°$ horizontal resolution with 47 vertical hybrid sigma-pressure levels from the surface to 0.01 hPa. The $1° \times 1°$ CDIAC fossil fuel and cement CO_2 emission data set for 2007 was used [*Andres et al*., 2011]. Sensitivity was determined by taking the difference between a simulation that had scale factors applied and a simulation without them (with identical initial conditions and fluxes), yielding CO_2 perturbations (ΔCO_2). Maps of ΔCO_2 are also shown in Figure 3, illustrating the spatial impacts, but, because some pixels are saturated using the selected color scale, the maximum and minimum values are not evident and instead

Table 2. Fraction of Emissions by Sector for Canadian Provinces and Territories in 2009 From Canada's *National Inventory Report*, Part 3 [2011][a]

Province	Residential[b]	Industrial	Utilities	Mobile	Other[c]
British Columbia (BC)	0.140	0.193	0.024	0.290	0.353
Alberta (AB)	0.077	0.237	0.261	0.113	0.313
Saskatchewan (SK)	0.081	0.122	0.327	0.152	0.318
Manitoba (MB)	0.213	0.176	0.014	0.438	0.159
Ontario (ON)	0.217	0.224	0.108	0.312	0.139
Quebec (QC)	0.169	0.215	0.008	0.418	0.190
New Brunswick (NB)	0.071	0.094	0.411	0.215	0.210
Nova Scotia (NS)	0.133	0.038	0.500	0.179	0.150
Prince Edward Island (PE)	0.337	0.055	0.000	0.466	0.142
Newfoundland and Labrador (NL)	0.095	0.108	0.104	0.245	0.449
Territories (Ter)	0.157	0.189	0.020	0.198	0.436
Canada	0.136	0.202	0.179	0.235	0.248

[a]Three significant digits are shown for simplicity, but more were used in the actual calculation.

[b]Residential here is actually the sum of residential and commercial.

[c]"Other" from the NIR accounts for a larger contribution than in EDGAR because of differences in the definitions of the sectors, related primarily to electric utilities.

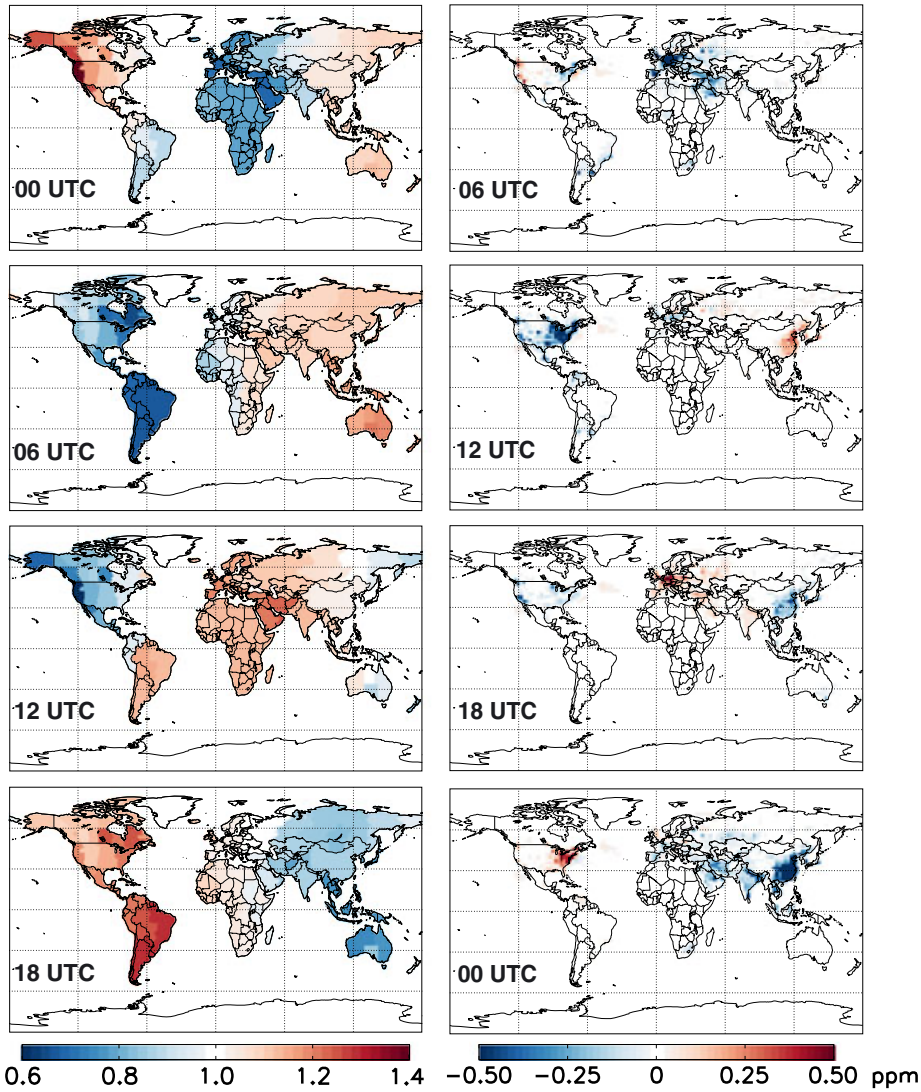

Figure 3. (Left) Global 0.25° × 0.25° dimensionless diurnal scale factor maps for 00, 06, 12, and 18 UTC. The boundaries between colored regions coincide with time zone boundaries, national borders, or Canadian provincial borders. Regions with a high proportion of emissions from on-road transportation have larger diurnal amplitudes. Both the minimum and the maximum can be seen to move westward throughout the course of a day. (Right) The CO_2 perturbation (ΔCO_2 determined as scaled – control) in the lowest atmospheric layer that results from applying the diurnal scale factors in a model for a typical December day. Because of the time lag of a few hours for the maximum atmospheric impact of the emissions scaling, the right panels are offset by 6 hours to obtain the best correspondence with the left panels. Impacts are largest over the highest-emitting regions (Eastern United States, Europe, and China), but, because some pixels are saturated (outside the color scale range) to illustrate the spatial effects better, the full magnitude of the impact in those regions cannot be determined accurately from this figure.

are dealt with in the Discussion. Offsetting the sensitivity maps by 6 h in Figure 3 gives a better match between the scaling factors and the ΔCO_2 perturbation in the atmosphere, which emphasizes that there is a time lag of a few hours between the most intense scaling and the maximum atmospheric perturbation, but the exact time lag will vary based on local transport factors.

2.2. Weekly Variability

[12] The same sectors with diurnal variability in Vulcan also have weekly variability. For these sectors, emissions on Saturday and Sunday are generally lower than on weekdays, with the greatest differences seen for on-road mobile followed by industrial emissions. Dimensionless factors were therefore determined for each sector on Saturday, Sunday, and weekdays, in which 1 corresponds to the weekly mean. These individual sector factors were used to calculate a sector-weighted total factor yielding 0.913268 for Sunday, 0.962927 for Saturday, and 1.024760 for weekdays, as shown in Table 3. A quick comparison with the diurnal scale factors from Figure 1, indicates that the scale factors for the weekly cycle are closer to 1 than the diurnal cycle.

[13] The reason for a weekly cycle in CO_2 emissions is entirely sociodemographic rather than geophysical and relates

Table 3. Weekday and Weekend Scale Factors for Five Sectors and the Weighted Total From Vulcan for the Contiguous United States in 2002[a]

	Residential	Commercial	Industrial	Utilities	Mobile	Total
Weekday	1.004859	1.003891	1.051292	1.026384	1.022697	1.024760
Saturday	0.984441	0.989275	0.873448	0.942249	1.023480	0.962927
Sunday	0.991269	0.991267	0.870090	0.925828	0.882269	0.913268

[a]The weekly mean has a value of 1.

to the customs and commercial schedules of the local population and thus will differ for different parts of the world. Different weekend definitions were not accounted for in the COFFEE implementation of weekly cycles [*Steinbach et al*., 2011], but satellite observations of the vertical column density of NO_2 (a short-lived tracer closely linked to anthropogenic emissions), averaged over the period 1996–2001 show different weekly cycles over many major cities of the world [*Beirle et al*., 2003]. U.S. and European cities, Mexico City, and others exhibited their primary minimum in NO_2 on Sunday, with slightly lower values on Saturday relative to the rest of the week, consistent with the traditional nonworking days in the West (related to Christian customs), as was seen in the Vulcan CO_2 emissions. For regions with other dominant religions, the weekly cycle was not as clear. NO_2 variability over Japanese and South Korean cities resembled that in the West, but many Middle Eastern cities (Cairo, Riyadh, Mecca, Abu Dhabi) had minimum NO_2 on Friday, consistent with their main day of rest, although Jerusalem had a minimum on Saturday. Over the past decade, numerous Middle Eastern countries have redefined their weekend from Thursday–Friday to Friday–Saturday, in order to balance the desire to synchronize their economies with their neighbors and the norms of international trade and yet respect Islamic religious traditions. *Gavison and Perez* [2007] provide a discussion on days of rest in various areas of the world. An updated online list of days of rest for various countries (http://en.wikipedia.org/wiki/Workweek_and_weekend) was used in this work.

[14] In the work of *Beirle et al*. [2003], Chinese cities did not show any weekly NO_2 cycle discernible from the noise, which was attributed to the fact that Chinese NO_x emissions were dominated by power plants and heavy industry operating throughout the entire week, whereas in many other parts of the world transportation emissions play a larger role. Although CDIAC (2011 update) indicates that China's CO_2 emissions doubled from 0.95 PgC in 2001 to 1.92 PgC in 2008, the proportion of emissions from road transportation has held roughly constant (~4%) over this period according to EDGAR v4.2 (road transportation emissions contribute ~26% in the United States according to Vulcan). However, Table 3 shows that industrial emissions make the largest contribution to the U.S. weekly cycle, so perhaps the lack of a weekly cycle in China's NO_2 relates to different industrial patterns during the time frame of that study.

[15] A weekly cycle in total CO_2 emissions for the 20 highest-emitting countries was determined by a weighted application of the U.S. scale factors for the four Vulcan sectors with weekly variability (and a constant factor of 1 for other emissions) to the proportion of the sector contribution to total emissions in EDGAR v4.2 (although the original Vulcan sector weighting is used for the United States). Countries not on the top 20 list were associated with a proxy country as in the previous section. In some cases, this meant that the weekly scaling was shifted by $1-2$ days from the proxy country, as in the case of Syria with a Saturday–Sunday weekend and its proxy Saudi Arabia with a Thursday–Friday weekend. Once again, Canadian provinces were each treated individually using the sector information from the *NIR* [2011] rather than the pan-Canadian value from EDGAR.

[16] All scale factors from this method were then gridded to $0.25° \times 0.25°$ using country and provincial masks at this resolution to give global scale factor maps for each day of the week (although Monday–Wednesday are identical), as shown in Figure 4. The sensitivity of surface atmospheric CO_2 to the weekly scale factors was determined using GEOS-Chem by an approach similar to that used in the previous section; however, here the sensitivity is determined using daily average CO_2 instead of an instantaneous value. This avoided selecting a single universal time for each map, since a single time obscures the spatial impacts of the weekly scaling by the diurnal cycle in meteorology, which systematically differs with longitude at a given time. Maps of the ΔCO_2 from the daily averages are shown in Figure 4, with some pixels saturated using the selected color scale range. These maps show more widespread, but less intense, perturbations than the diurnal impact maps. The maximum intensity of the perturbations is reviewed in the Discussion.

2.3. Variability in Per Capita Distributions for Canada

[17] The gridded CDIAC emission data set [*Andres et al*., 2011] uses population for spatially distributing emissions within a country. Although this may be reasonable for many countries, the reliability of this approach decreases for larger countries (and finer spatial scales), because regions could differ widely in terms of their energy-intensive industries, electricity generation methods, transportation patterns, heating/cooling requirements, or even overall standard of living. Per capita differences in the United States were identified by *Pétron et al*. [2008]. *Zhou and Gurney* [2011] demonstrate deviations from the national mean per capita CO_2 emissions for the United States based on Vulcan, and *Gurney et al*. [2009] show the impact of these differences on an atmospheric CO_2 simulation, indicating annually averaged differences of up to ± 1.8 ppm at 850 hPa relative to a simulation with a constant per capita emissions. The most densely populated parts of the United States, particularly the West Coast, East Coast northeast from Washington D.C., and the area of Chicago and environs, were associated with lower atmospheric CO_2 in the simulation using Vulcan (indicative of per capita emissions below the U.S. mean), whereas most other parts of the United States had higher CO_2 concentrations. Other analyses comparing modeled atmospheric CO_2 based on Vulcan emissions relative to a simulation using a uniform per capita emission distribution [*Corbin et al*., 2010, *Schuh et al*., 2010] were in general agreement with

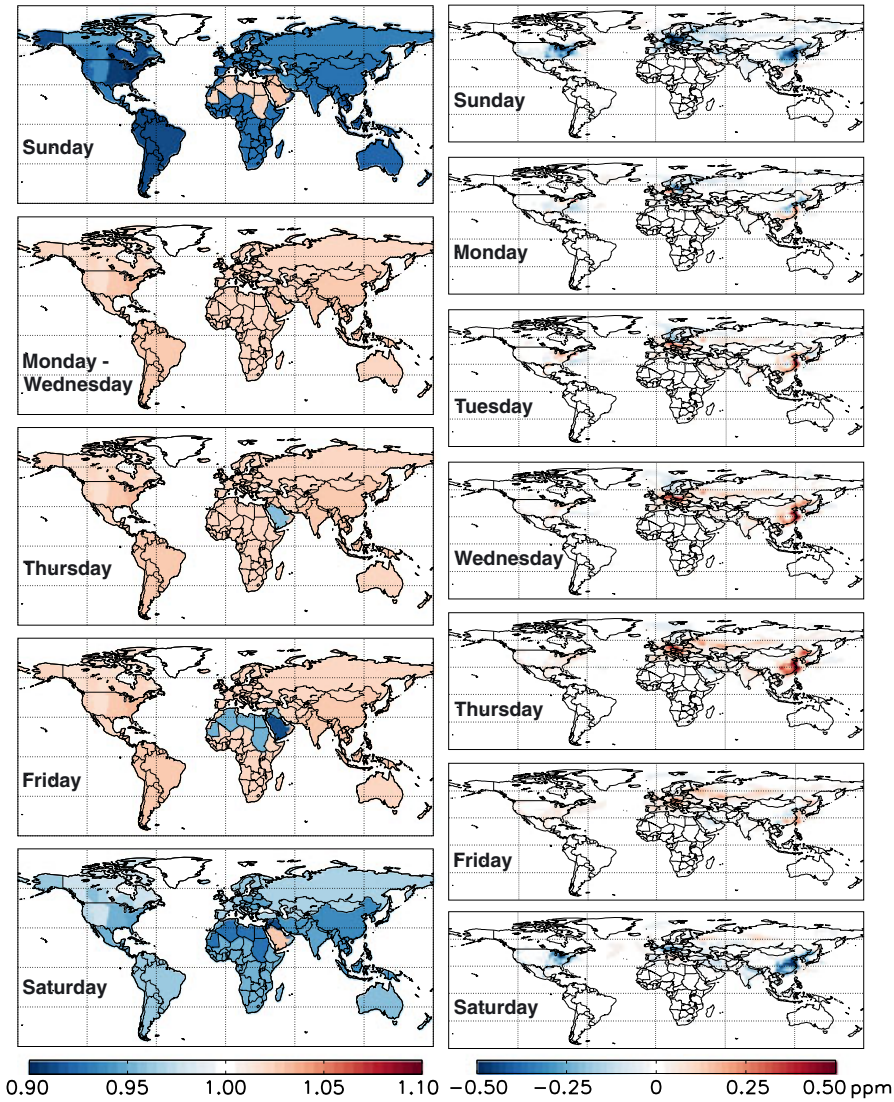

Figure 4. (Left) Global $0.25° \times 0.25°$ dimensionless weekly scale factor maps for Sunday, Monday Wednesday, Thursday, Friday, and Saturday, accounting for the different definitions of the weekend around the world. (Right) The daily-averaged CO_2 perturbation (ΔCO_2) in the lowest atmospheric layer that results from applying the weekly scale factors in a model for a typical December week. As with the diurnal scale factors, the impacts are greatest over the high-emitting regions (where some pixels are saturated), but the impacts of the weekly variability are less intense and more dispersed.

the earlier result but also showed localized differences of as much as ± 5.0 ppm, most often near urban areas.

[18] Canada is the world's second largest country, with an area of 9.98×10^6 km^2 and the seventh highest fossil fuel CO_2-emitting country (according to CDIAC for 2008). It is responsible for ~2% of global emissions, so misrepresenting the spatial distribution of fossil fuel CO_2 emissions within Canada could result in major spatial biases in global model simulations, which would be less significant for smaller countries. Such CO_2 emission biases could impact inverse modeling estimates of terrestrial biospheric CO_2 fluxes. Canada's *NIR* [2011] provides information on greenhouse gas emissions from each province, each province's population, and the breakdown of contributions from different sectors and subsectors (Part 3, Appendices), but the emission values are not distributed spatially for use in atmospheric CO_2 modeling. In $1° \times 1°$ province area masks, the fraction of emissions from each province in the gridded CDIAC (2011 update) and ODIAC v3.0 data relative to the national total (excluding emissions from international shipping and aviation) was determined and compared with the NIR provincial fractions (excluding emissions from agriculture, waste, or land use and land use change from the calculation). Provincial populations and their contribution to national emissions from the NIR, along with scale factors determined from comparing NIR/CDIAC and NIR/ODIAC, are shown in Table 4. Table 5 shows the annual per capita provincial CO_2 emissions from various sectors and subsectors identified in the *NIR* [2011]. Canada's national per capita CO_2 emissions are 4.39 Mg C person^{-1} yr^{-1}, with Alberta and Saskatchewan well above the national mean (13.68 and 11.94 Mg C person^{-1} yr^{-1}, respectively), and

Table 4. Population for Canadian Provinces and Territories Along With the Fraction of National Emissions That the Province Contributed in 2009, Determined From Part 3 of Canada's *National Inventory Report* [*NIR*, 2011][a]

Province	Population (thousands)	Fraction of Canadian population	Fraction of Canadian emissions	NIR/CDIAC	NIR/ODIAC
British Columbia (BC)	4,460	0.132266	0.094649	0.86865	1.38346
Alberta (AB)	3,671	0.108867	0.339483	3.77577	1.18719
Saskatchewan (SK)	1,029	0.030516	0.083026	2.26296	1.16052
Manitoba (MB)	1,220	0.036180	0.021218	0.52631	0.433737
Ontario (ON)	13,065	0.387456	0.256458	0.68262	0.916361
Quebec (QC)	7,828	0.232147	0.116052	0.45671	0.685165
New Brunswick (NB)	749	0.022212	0.030996	0.94641	0.367976
Nova Scotia (NS)	939	0.027847	0.057934	1.28426	1.70118
Prince Edward Island (PE)	141	0.004181	0.002362	0.30150	1.070118
Newfoundland and Labrador (NL)	508	0.015065	0.015240	0.66289	1.29663
Territories (Ter)	110	0.003262	0.003229	1.12138	0.519725
Canada	33,720	1	1	0.93040[b]	0.90035[b]

[a]Also shown are scale factors that could be applied to CDIAC and ODIAC to match these values, determined as the NIR fraction divided by the 2008 CDIAC or ODIAC fraction.

[b]Canada ratios differ from 1 primarily because 2009 NIR values were used with 2008 CDIAC and ODIAC values, and Canada's CO_2 emissions declined in 2009. Using 2008 NIR values gives NIR/CDIAC = 0.99065 and NIR/ODIAC = 0.95866, where the remaining difference from 1 likely is due to defining the Canada – United Stattes border with a mask of finite horizontal resolution ($1° \times 1°$).

Quebec, Prince Edward Island, Manitoba, Ontario, and British Columbia below (2.19–3.14 Mg C person^{-1} yr^{-1}), whereas Newfoundland, Nova Scotia, New Brunswick, and the combined territories are near the mean (4.34–6.12 Mg C person^{-1} yr^{-1}).

[19] The high per capita emissions for Alberta and Saskatchewan are the result mainly of the predominant use of coal for the electricity supply (74% and 63%, respectively). However, emissions from fossil fuel production and refining (18.6%) and from oil and gas extraction (12.6%) and fugitive emissions from oil and natural gas (6.2%) in Alberta also play a major role. This is also true for Saskatchewan to a slightly lesser extent (fossil fuel production and refining contributing 13.5%, oil and gas extraction 7.8%), although nonroad mobile emissions (8.7%), presumably related to farming, also contribute at a proportion well above other provinces. Saskatchewan (followed by Alberta) also has the highest per capita emissions from on-road transport according to Table 5. The lower per capita emissions of Quebec and Manitoba arise primarily because 96% and 98% respectively of their electricity was generated using hydroelectricity, which does not directly emit CO_2. Per capita CO_2 emissions in Ontario were almost as low as those in Quebec and Manitoba, related to the fact that 56% of the Ontario electricity supply was from nuclear energy, 27% from hydroelectricity, and 1.5% from other renewable energy (wind, solar, geothermal) sources in 2009 [*NIR*, 2011]. The high use of coal and major industrial and

Table 5. Per Capita Emissions by Sector (MgC/yr)[a] for Canadian Provinces, the Territories, and the National Mean in 2009, Determined From Part 3 of Canada's National Inventory Report [2011]

	BC	AB	SK	MB	ON	QC	NB	NS	PE	NL	Ter	Can
Energy	3.01	12.94	11.59	2.48	2.61	1.98	6.01	5.58	2.46	4.40	4.34	4.10
a. Stationary Combustion Sources												
Electricity and Heat	0.07	3.57	3.90	0.04	0.32	0.02	2.51	2.82	0.00	0.46	0.09	0.79
Fossil Fuel Production and Refining	0.38	2.55	1.61	0.00	0.12	0.12	0.92	0.37	0.00	0.94	0.06	0.50
Mining & Oil and Gas Extraction	0.11	1.73	0.94	0.03	0.01	0.02	0.02	0.01	0.00	0.42	0.81	0.25
Manufacturing	0.37	0.76	0.14	0.31	0.32	0.23	0.45	0.15	0.12	0.02	0.00	0.34
Construction	0.00	0.01	0.01	0.02	0.01	0.01	0.00	0.01	0.01	0.00	0.00	0.01
Commercial & Institutional	0.18	0.41	0.51	0.32	0.27	0.27	0.26	0.48	0.37	0.28	0.46	0.29
Residential	0.25	0.63	0.46	0.23	0.37	0.10	0.17	0.27	0.47	0.14	0.22	0.31
Agriculture & Forestry	0.00	0.03	0.06	0.01	0.02	0.01	0.01	0.02	0.03	0.00	0.00	0.02
b. Transport												
Domestic Aviation	0.08	0.10	0.05	0.11	0.04	0.03	0.04	0.07	0.03	0.11	0.76	0.06
Road Transport	0.91	1.54	1.81	1.13	0.91	0.92	1.32	1.01	1.16	1.09	0.86	1.04
Rail	0.03	0.21	0.11	0.05	0.02	0.02	0.08	0.04	0.01	0.02	0.00	0.05
Domestic Marine	0.12	0.00	0.00	0.00	0.01	0.04	0.10	0.12	0.14	0.24	0.00	0.04
Off-Road	0.24	0.52	1.03	0.20	0.16	0.17	0.08	0.18	0.14	0.40	1.04	0.25
Pipelines	0.05	0.11	0.59	0.02	0.02	0.01	0.00	0.02	0.00	0.00	0.01	0.05
c. Fugitive Sources												
Oil and Natural Gas	0.20	0.80	0.37	0.01	0.01	0.01	0.06	0.02	0.00	0.28	0.01	0.14
Industrial Processes	0.12	0.74	0.37	0.10	0.31	0.21	0.10	0.04	0.00	0.04	0.01	0.28
Waste	0.00	0.00	0.00	0.00	0.00	0.00	0.00	0.00	0.02	0.00	0.00	0.00
Total[b]	3.14	13.68	11.94	2.57	2.90	2.19	6.12	5.64	2.48	4.44	4.34	4.39

[a]1 Mg = 1 Tonne

[b]Total is based on the total in the NIR, therefore Total ≈ Energy + Industrial Processes + Waste, but can differ slightly due to the number of significant digits quoted for the total, sector or sub-sector.

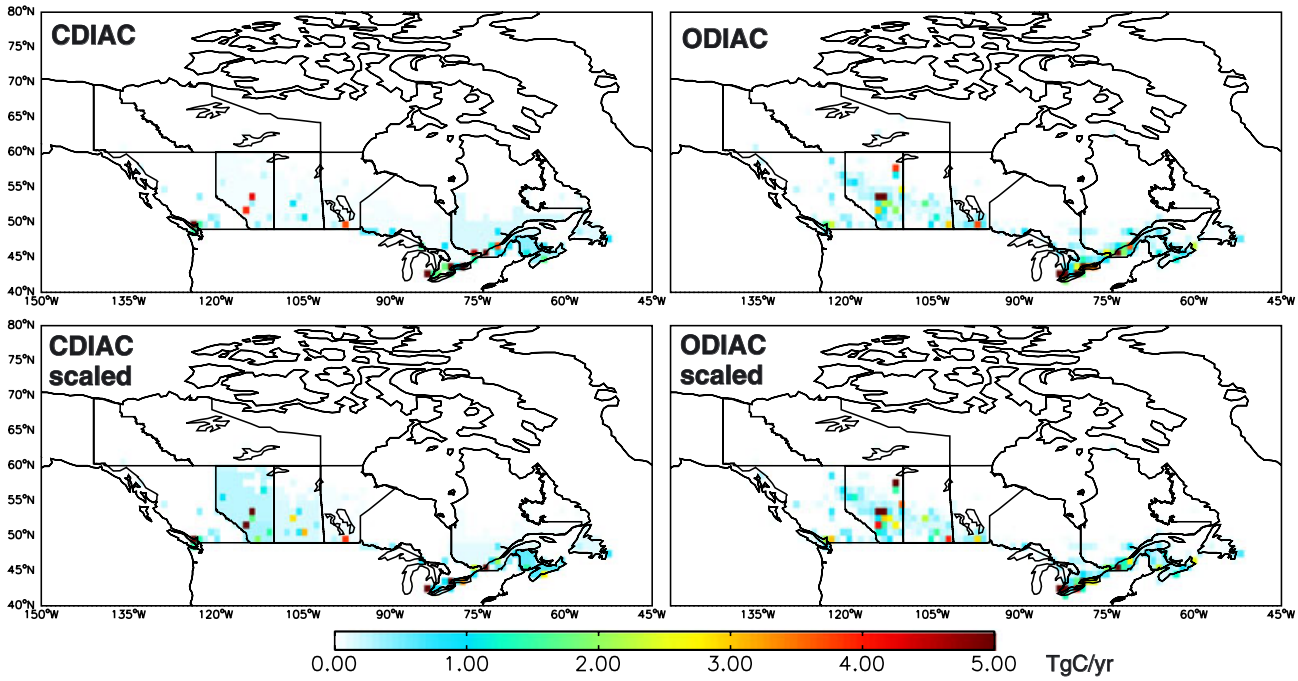

Figure 5. CDIAC and ODIAC CO_2 emissions for Canada at $1° \times 1°$ and the emissions scaled using provincial scale factors (Table 4) based on per capita emissions from Canada's *National Inventory Report* [2011]. Changes in ODIAC are less pronounced than CDIAC, suggesting that nightlights (and the point source list) give a better representation than a purely population-based approach.

agricultural contributions in Alberta and Saskatchewan and the use of non-CO_2-emitting electricity generation in Quebec, Manitoba, and Ontario highlight a limitation of the population-based distribution of emissions at the national level rather than the provincial level. Application of the scale factors in Table 4 to CDIAC and ODIAC is shown in Figure 5. The fact that the ODIAC nightlights- and point-source-based emission data set has scale factors closer to 1 and changes in Figure 5 are less pronounced suggests that this approach is an improvement relative to CDIAC, but it is still subject to limitations in accounting for emissions from the petroleum industry and farm vehicles or diverted emissions from non-CO_2-emitting electricity generation. Errors with the locations and the magnitude of point source emissions in ODIAC would not necessarily be highlighted in this approach. The approach used here is most effective for evaluating the province-scale values and provides some suggestion of the validity of the spatial distribution within a province, but it does not evaluate the accuracy of ODIAC spatial distributions at high resolution; however, some of the largest Canadian CO_2-emitting point sources located in sparsely populated areas (Fort McMurray, Alberta; Nanticoke, Ontario; and Estevan, Saskatchewan) appear reasonably located in the ODIAC distributions, although they are absent in the CDIAC distributions (Figure 5).

3. Results and Discussion

[20] The TIMES scale factor maps developed in this work can be used to represent the diurnal and weekly scale variability in anthropogenic CO_2 emissions by applying them to CO_2 emission data from CDIAC, ODIAC, or EDGAR when used in CO_2 transport models. Previous work has estimated that the diurnal variation resulting from Vulcan emissions can have an impact of nearly ± 3.0 ppm for select locations, relative to constant daily emissions [*Corbin et al.*, 2010], but in those tests the diurnal effects were not completely isolated from other factors. Direct studies of the diurnal cycle of CO_2 emissions for individual cities have also been conducted [*Vogt et al.*, 2005, *Kühlwein et al.*, 2002], but other work has focused on the change in atmospheric CO_2 concentrations from the diurnal cycle in fossil fuel CO_2 emissions on local scales [*Coutts et al.*, 2007; *Vogel et al.*, 2010].

3.1. Impact on Surface Atmospheric CO_2

[21] In this section, we investigate the impact of the TIMES scaling factors on surface atmospheric CO_2 distributions by taking the difference between simulations with the scaling applied and without. Figures 3 and 4 show that the spatial patterns of the impacts of the diurnal and weekly scaling factors are largest over high-emitting regions, including the Eastern United States, Europe, and China, and moderate over some other regions (U.S. West Coast, the Middle East, India, Japan), but negligible over the majority of the globe. Some pixels are saturated with the chosen color scale (to illustrate better the spatial effects), so the absolute magnitude at a given location within the high-emitting areas is not evident. Figure 6 illustrates the impact of diurnal and weekly scaling over a 60-day period from a GEOS-Chem model simulation, based on two $2° \times 2.5°$ surface grid boxes from each of the regions with the largest ΔCO_2 perturbations, corresponding to New York City, Berlin, and Beijing, as well as two other major cities, Los Angeles and Tehran, from regions of moderate perturbations. The left column shows total CO_2 with both temporal scale factors applied

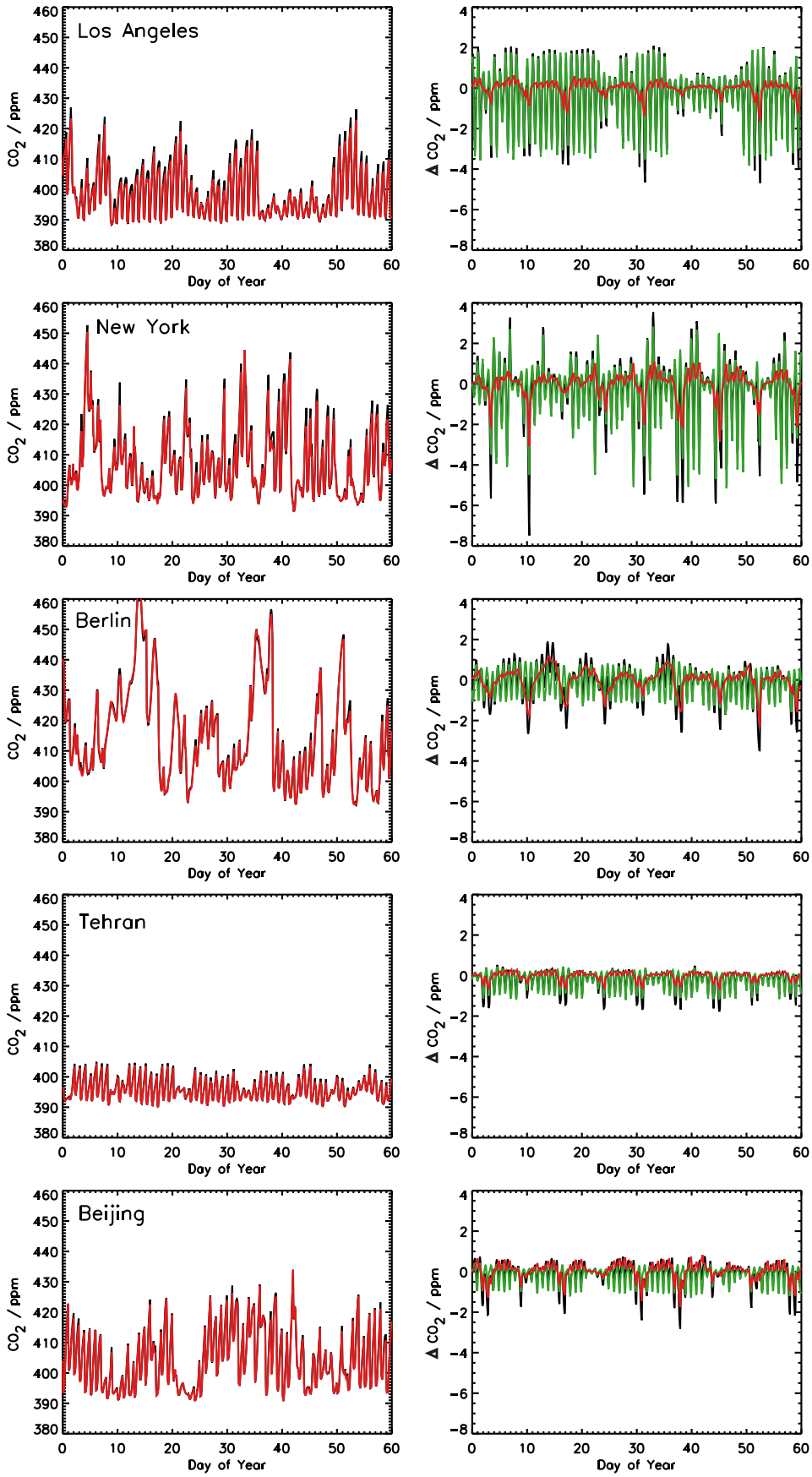
Los Angeles
New York
Berlin
Tehran
Beijing
CO2 / ppm
Δ CO2 / ppm
Day of Year

Figure 6

and without any temporal scaling. The differences appear minor relative to the background of about 395 ppm CO_2 and the observed variability, which is mainly related to synoptic scale transport; however, the right column shows the residuals or the ΔCO_2 perturbations as a function of time for diurnal scaling, weekly scaling, and combined (weekly + diurnal) scaling, illustrating that the impact is significant at select locations. The contribution from the weekly scaling (~0.5–3.0 ppm) is smaller but more long-lived than the diurnal scaling (~1–5 ppm), as evidenced by the sharper and more regular diurnal fluctuations. Interestingly, the weekly perturbations also display a faint diurnal cycle related to the combination of synoptic transport with higher/lower constant daily emissions.

[22] The combined weekly and diurnal perturbations are characterized by a period of 1 week, in which the most prominent features occur because of the coincidence of the weekly minimum (usually Sunday) with the diurnal minimum and can yield perturbations as large as ~8 ppm for New York City, ~5 ppm for Los Angeles, ~4 ppm for Berlin, ~3 ppm for Beijing and just under ~2 ppm for Tehran. It is presumed that the differences between these locations relate to the absolute magnitude of emissions from the city, the amplitude of the diurnal and weekly scale factors, the local and regional meteorological effects, and the size of the area selected (a $2^\circ \times 2.5^\circ$ grid box is ~$222 \times 250\,km^2$ at these latitudes). Although cities are actually smaller than a single grid box, two boxes were used rather than one because some cities straddle the boundary of two boxes, and a uniform approach was desired for all cities. If a model with higher horizontal resolution was used, the city area could be better defined, likely leading to more intense perturbations.

[23] The combined diurnal and weekly scaling impacts in the range of ~1.5 to ~8 ppm for large cities of the world can be contrasted with the accuracy (~0.2 ppm) and precision (~0.1 ppm) of flask [*Conway et al.*, 1994] and continuous in situ CO_2 [*Worthy et al.*, 2003] measurements. Both measurement types are commonly used in CO_2 inverse modeling and data assimilation systems, in which the fossil fuel CO_2 is often treated with zero error in order to optimize terrestrial biospheric or oceanic CO_2 fluxes. Although these inversions use predominantly background observations to minimize such errors (or inflate the observation errors to account imperfectly for uncertainties like this), as anthropogenic emissions increase, as measurement network coverage expands, and as the desire to constrain fluxes at finer spatial and temporal scales grows, the inclusion of nonbackground sites and reduction of biases from fossil fuel emission inventories will be of greater importance.

3.2. Impact on XCO_2

[24] Satellite missions or instruments that measure CO_2 using near-infrared (NIR) or shortwave infrared (SWIR) solar reflectance from the Earth's surface commonly provide a column-averaged CO_2 mixing ratio referred to as XCO_2. These observations have vertical sensitivity spanning the entire atmospheric column, including the boundary layer. The sensitivity is nearly uniform vertically throughout the troposphere, then decreases above, with the detailed vertical sensitivity described by a column averaging kernel vector $\boldsymbol{a}_{CO2}$ [*Yoshida et al.*, 2011]. As a result, the behaviour of XCO_2 differs from that of boundary layer CO_2, but XCO_2 still contains information about CO_2 near the surface for studying sources and sinks [*Olsen and Randerson*, 2004]. Satellites in sun-synchronous orbits have a fixed local equator-crossing time for the ascending and descending nodes of each orbit, such that the daylight equator-crossing times are 10:00 for SCIAMACHY [*Buchwitz et al.*, 2007], 12:48 for GOSAT [*Yoshida et al.*, 2011], and ~13:30 for OCO-2 [*Crisp et al.*, 2004, 2012] and the proposed CarbonSat [*Bovensmann et al.*, 2010], so all observations are within minutes of this local time.

[25] *Olsen and Randerson* [2004] compared the impacts of the biospheric diurnal cycle on surface CO_2 and XCO_2 by using model simulations. Here, we will compare the impacts of our TIMES fossil fuel scaling on XCO_2 and contrast these results with those of surface CO_2 from section 3.1. Figure 7 shows the perturbations due to the diurnal and weekly scaling factors on XCO_2 calculated using an empirical representation of a mean GOSAT column averaging kernel based on the work of *Yoshida et al.* [2011]. As in Figures 3 and 4 for surface CO_2, Figure 7 illustrates the spatial distribution with limited information about the exact magnitude of the impact, because some pixels are saturated with the color scale used. Although the color scale range for XCO_2 has been reduced by a factor of 5 relative to surface CO_2, the spatial patterns of the perturbations have some similarities, although some important differences are evident too. For example, the relative impact over the north Atlantic due to the US East Coast is more evident for XCO_2 from both diurnal and weekly scaling, and, unlike the case for surface CO_2, the spatial patterns are slightly more complex, with more frequent "dipoles" consisting of negative and positive lobes in a given region. These dipoles likely result from the transport of air with increased or decreased CO_2 above the surface level near an area where the surface impact has the opposite sign. A qualitative comparison seems to indicate that the impacts from the weekly variability are actually more intense than the diurnal variability, in contrast to the overall case for surface CO_2, for which the reverse was true. Figure 8 shows the impacts on XCO_2 for the same major cities as in Figure 6, but with the range of the y-axis reduced relative to the surface CO_2 figure. This confirms that the perturbations from weekly variability are typically larger than those from the diurnal variability, which is best illustrated for Beijing.

[26] Although the XCO_2 impacts are generally less than for surface CO_2, they are significant relative to the 0.3% (~1.0 ppm) precision targeted by OCO-2 [*Crisp et al.*,

Figure 6. (Left) Surface-level atmospheric CO_2 at selected major cities with both weekly and diurnal scaling applied (red) and the unscaled control simulation (black) over a 60-day period. (Right) The residuals determined as weekly scaling minus control (red), diurnal scaling minus control (green), and combined temporal scaling minus control (black). These residuals give a measure of the temporally dependent impact or ΔCO_2 perturbation. The combined impact is highest for New York City, often reaching the range of 5−8 ppm.

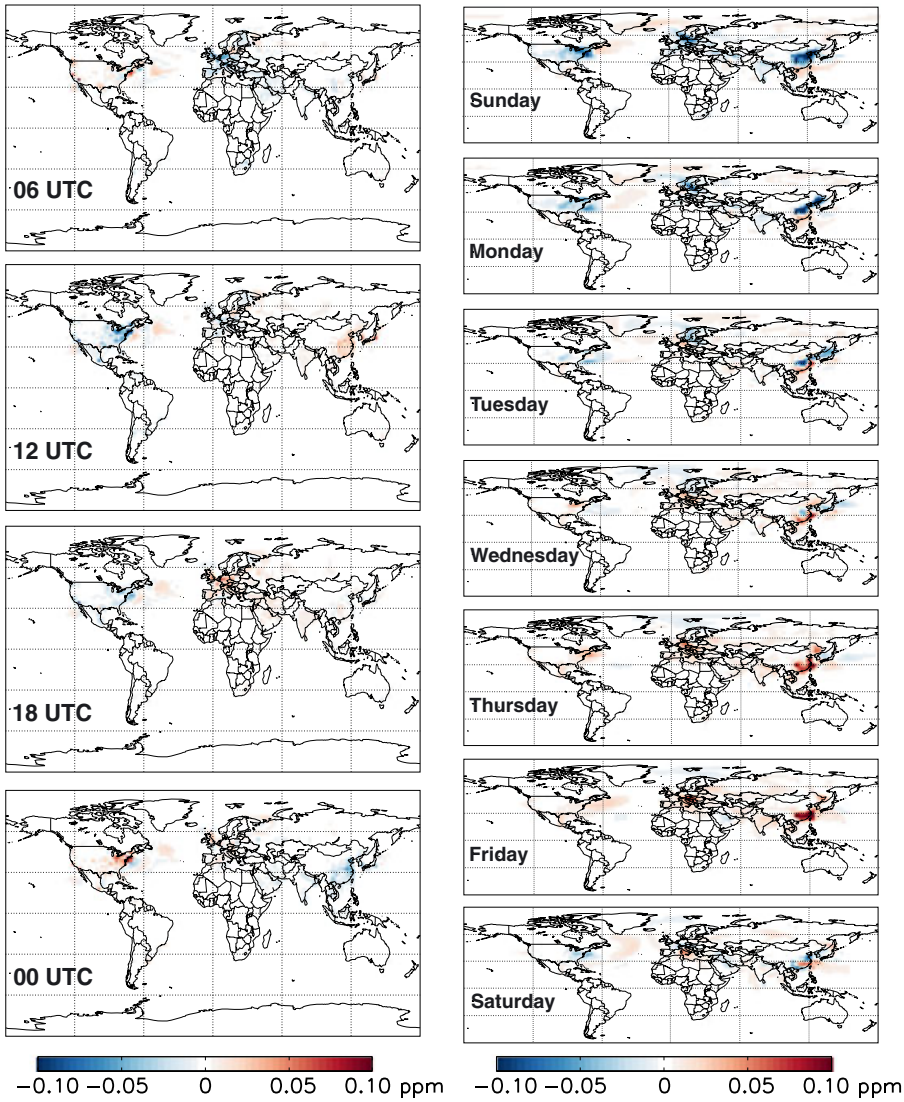

Figure 7. The column-averaged CO_2 (XCO_2) perturbation (ΔXCO_2 determined as scaled – control) from applying (left) the diurnal scale factors in a model for a typical December day and (right) the weekly scale factors for a typical December week.

2004, 2012] and 0.25 ppm precision of satellite validation data from the Total Carbon Column Observing Network (TCCON) [*Wunch et al*., 2011]. Hence, we recommend that these modes of temporal variability not be neglected in systems designed for assimilating satellite XCO_2 data. The larger contribution from weekly variability for XCO_2, in contrast to the situation for surface CO_2, with the diurnal cycle having a larger impact, could perhaps have been foreseen considering that XCO_2 consists of a vertically integrated signal from air that was in contact with the surface over a larger span of time. It is also consistent with the findings of *McKain et al*. [2012], who, in an assessment of ground-based CO_2 observations for verification of urban greenhouse gas emissions, state that "integrated column measurements of the urban dome of CO_2 from the ground and/or space are less sensitive than surface point measurements to the redistribution of emitted CO_2 by small-scale processes and thus may allow for more precise trend detection of emissions from urban regions."

3.3. Limitations, Uncertainties, and Future Directions

[27] The approach of producing temporal (and spatial) scale factor maps, rather than a new set of emission data files (such as the COFFEE approach) was chosen for this work. The primary reason for this rather than a multiyear, hourly data set is that the scale factor approach provides the variability in modular form, because some users might be interested in per capita scaling but not temporal scaling (or vice versa) or even interested in weekly scaling but perhaps not diurnal scaling (or vice versa).

[28] However, a drawback of the modular scale factor approach is that it makes annual assumptions about the contributions from different sectors, which obviously do change with season. Although the first-order seasonal effect is now accounted for in CDIAC or ODIAC totals, the second-order sector proportional change, which affects the scale factors, is not accounted for in our work, effectively ignoring some of the information available from Vulcan. We have also

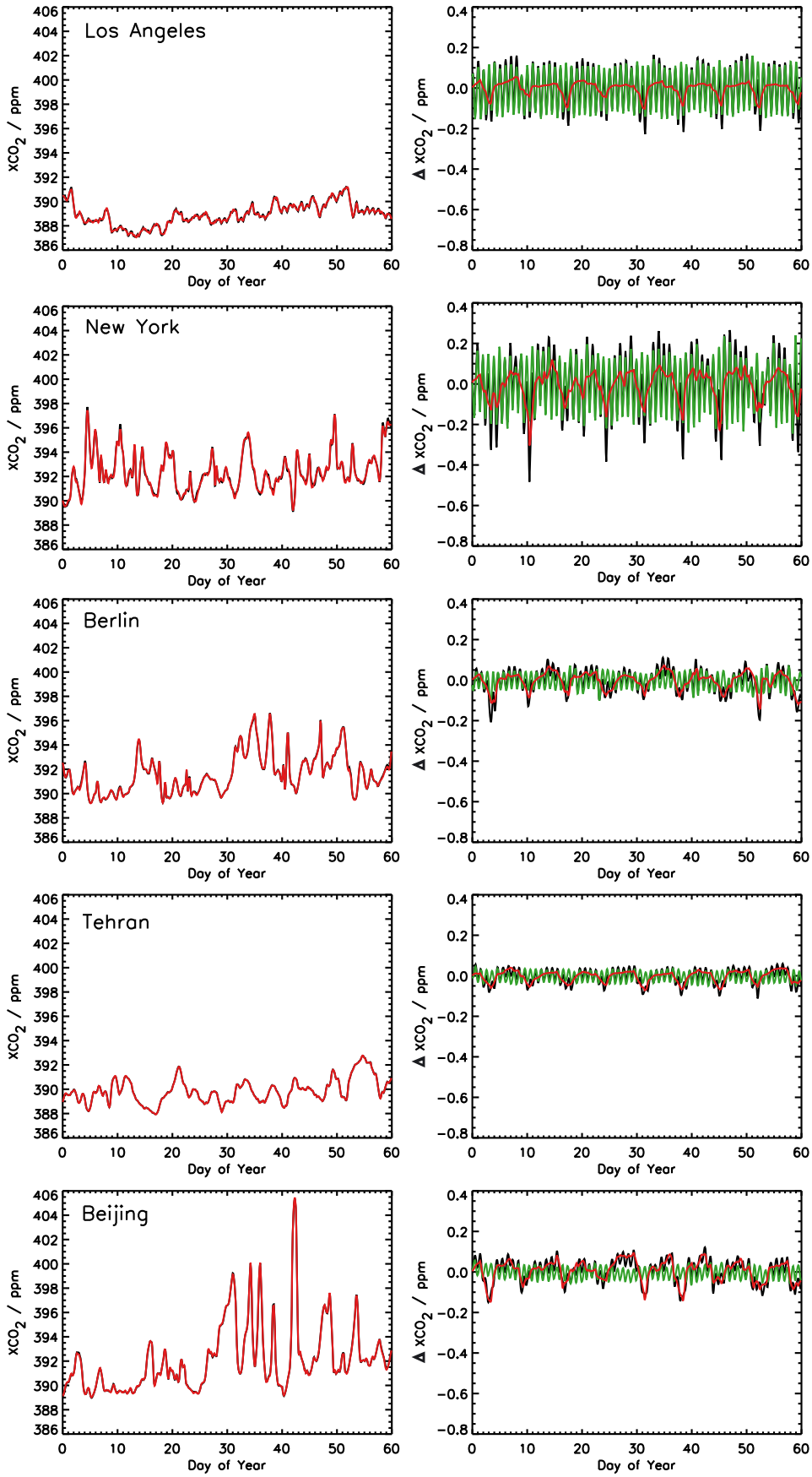

Figure 8. Same as Figure 6, but for XCO_2 and ΔXCO_2. The combined impact is highest for New York City, often reaching the range of 0.4–0.5 ppm.

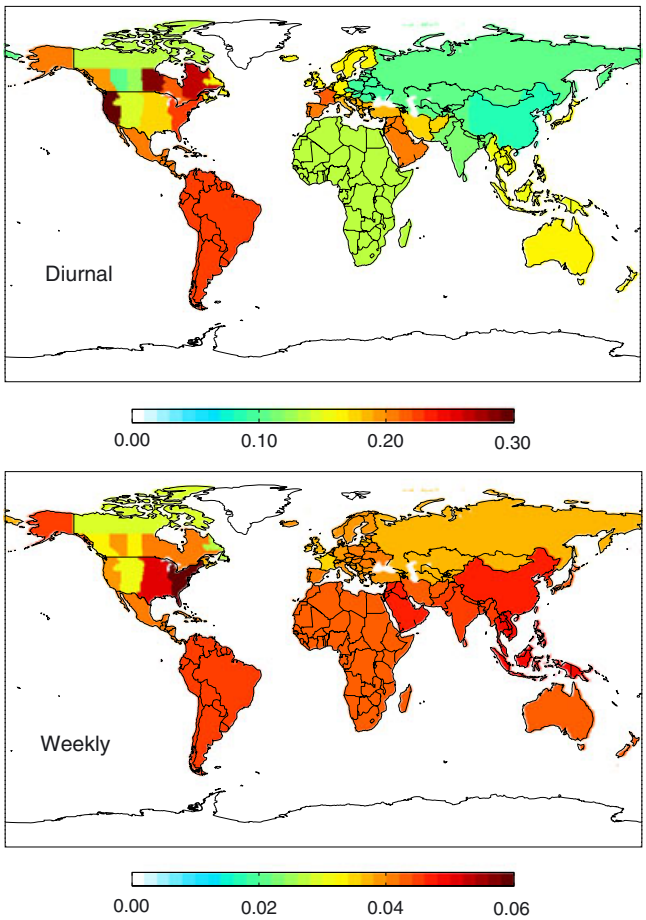

Figure 9. Maps of the standard deviation of the dimensionless diurnal (top) and weekly (bottom) scale factors, which can be used as a measure of uncertainty but do not account for all systematic errors.

applied a single mean diurnal cycle (as mentioned earlier) rather than different weekday and weekend diurnal cycles. Real diurnal cycles for emissions on weekdays and weekends will differ. Weekends are expected to have a largely dampened bimodal (morning/afternoon rush hour) peak in the diurnal cycle because of transportation emissions relative to weekdays and should generally exhibit an increase later in the day relative to the nighttime minimum.

[29] Another significant issue is a temporal bias in the weekly cycle that results for time zones that differ from the zone selected for the day-of-week change. In global modeling work, this will typically be UTC. This problem arises because the weekly scaling map changes at midnight UTC (or another chosen time zone) for the whole globe rather than for the local time. This would be negligible for Berlin, resulting in a phase shift of +1 hour, but the New York weekly cycle would have a phase shift of −5 hours and Beijing +8 hours. For regional modeling (or global modeling with a regional focus), a different time zone could be selected for the day change, which would greatly reduce this effect for the desired locality. However, we note that the diurnal cycle has a larger instantaneous impact than the weekly cycle, where the impact from the weekly cycle is realized as persistently lower weekend emissions over a period of 48 hours, so a cycle with a realistic amplitude, but a phase shift of a $5-8$ hours, is expected to be better than the complete absence of weekly variability.

[30] An alternative approach to deal with the second-order effects (interaction among seasonal, weekly, and diurnal cycles) would be to produce a set of 12×7 weekly scale factors or $12 \times 7 \times 24$ diurnal scale factors to account for these differences, which could be explored in the future. Combining the weekly and diurnal cycles into 7×24 maps would remove the phase-shift issue mentioned above. It should also be noted that regridding the scale factors to coarser model horizontal resolution (as in our tests) will result in lowering the amplitude of weekly/diurnal cycles next to regions of no scaling such as oceans, although total emissions will still be properly conserved.

[31] The discussion above highlights the fact that derivation of the TIMES and Canadian spatial scale factors includes a number of approximations and simplifications. The application of more detailed bottom-up methods, such as that used in Vulcan, would likely provide better estimates of CO_2 emissions for high spatial and temporal scales, but these are very labor-intensive undertakings, which to date have been performed for very few countries and only in select years (i.e., United States in 2002). Scale factors allow for immediate application to new releases of inventories such as CDIAC or ODIAC, which occur every year based on annual UNFCCC updates or similar data, with a typical time lag of about 2.5 years (i.e., 2009 emissions distributions are provided no earlier than mid-2012). If a new product were to be produced each time (like COFFEE) instead of scale factors, the additional step required would increase the time lag. The time lag for availability of an emission data product is an issue in the potential application of inventories in future operational CO_2 data assimilation systems that could run in near-real time. Additionally, if the objective of such systems was to quantify anthropogenic emissions, using the fossil fuel emission data only as an a priori estimate, this would be consistent with practical approximations such as scale factors.

[32] Uncertainties in the temporal distributions of fossil fuel CO_2 emissions for the EDGAR v3.2 provisional data or COFFEE have not been quantified, nor to date have uncertainties in the spatial distributions of emissions in CDIAC, ODIAC or EDGAR (beyond the country scale), although uncertainties in the spatial distributions have been discussed by *Andres et al*. [2012]. Quantifying uncertainties in these data products or the scale factors developed here is a challenge. As with the scale factors themselves, their uncertainties will be nonuniform across the globe because of different energy generation methods and usage patterns. A possible method to estimate the uncertainty of the scale factors is to assign the uncertainty related to the level of scaling applied, so, for regions where the scaling amplitude is large, there are larger uncertainties, and, for regions where scale factors are closer to unity, the uncertainties are low. Figure 9 shows maps of the standard deviation of the scale factor values over one cycle (0–23 values for diurnal, 1–7 values for weekly). The 1σ uncertainties are from 0.07 to 0.30 for diurnal scaling range and from 0.03 to 0.06 (dimensionless scale units) for weekly scaling. It should be noted, however, that these uncertainty estimates are incomplete, insofar as they relate only to the intensity of scaling and do not account for systematic errors in the method or the input data.

[33] Another approach to estimating uncertainties could be developed later through comparison of simulated CO_2 using the scaling with measurements, perhaps using direct fossil fuel CO_2 tracer methods such as $^{14}CO_2$ [*Turnbull et al.*, 2009; *Levin et al.*, 2011; *Miller et al.*, 2012], because these methods are not subject to the uncertainties in CO_2 fluxes from other components (biosphere, oceans) of the earth system, although they still have their own limitations. It is possible that these studies could identify weaknesses in the current approach, for example, the proxy country groupings, which would require an update to the scale factors, but these changes are expected to be a higher-order correction to the imposition of spatial and temporal variability in emissions that was completely absent in the past.

[34] The use of Canada's NIR for adjusting Canadian emissions for per capita differences is expected to be an improvement upon the current CDIAC and ODIAC emission values, because of the large per capita variation across the country. An evaluation of the sensitivity of atmospheric CO_2 to the spatial scaling, or its impact on CO_2 inversions, will be left for future work. Allocation of emissions per capita is a challenging problem and depends heavily on the spatial scales desired. Although our scale factors now change the relative proportion of the emissions from one province to the next, we have not altered the distribution at finer spatial scales. *Hoornweg et al.* [2011] indicated that per capita urban emissions are lower than from suburban or rural areas in developed countries because of factors such as urban public transit and smaller dwellings, whereas in developing countries per capita emissions are typically higher in urban areas compared with rural areas and correlate with the general standard of living. That work also showed that, even within a single metropolitan area (or a single neighbourhood), there is a wide range of variability in per capita emissions, but properly accounting for these differences is beyond the scope of this work and is probably better accomplished using bottom-up methods, at least for the time being.

[35] Another promising approach to developing fossil fuel emission inventories with improved spatial and temporal information is the development of a Fossil Fuel Data Assimilation System (FFDAS) [*Rayner et al.*, 2010]. With enough sophistication in such a system, it is theoretically possible to input information to address all of these issues and also estimate uncertainties in emissions, but the current FFDAS is still in its infancy. A modest redistribution of emissions based on per capita differences between provinces, as carried out here, will potentially make a significant difference in continental-scale CO_2 distributions over short time scales, whereas further improvements to represent subprovincial scales better are more challenging, but are expected to have less impact anyway, because of the tendency for sharp pollution gradients to diffuse rapidly, while the transport of larger pollution-enhanced air masses between continents is common.

4. Summary and Conclusions

[36] CO_2 emissions from fossil fuel combustion in CDIAC, ODIAC, and EDGAR currently do not include variability in emissions over the course of a week or throughout the day, but inverse modeling and data assimilation systems that use these inventories often deal with measurements subject to variability on these time scales, such as weekly flask CO_2 measurements or satellite observations of CO_2 from a sun-synchronous orbit corresponding to a single point in the diurnal cycle. Measurements from periodic sampling and the increasing use of continuous in situ measurements both increase the need for proper modeling of weekly and diurnal cycles.

[37] Using the Vulcan v2.0 emission data product for the United States and emission sector information from EDGAR v4.2 for the 20 highest-emitting countries, along with information on weekly cycles from satellite observations of NO_2 and other sources, we derive scale factor maps that can be applied to the global inventories to represent weekly and diurnal variability. We refer to this new product as TIMES (Temporal Improvements for Modeling Emissions by Scaling). Because Canada's *NIR* [2011] provides information on the differences between the contributions from different sectors among the Canadian provinces, we use provincial information for Canada rather than EDGAR national sector contributions.

[38] Surface atmospheric impacts of the combined diurnal and weekly scaling were determined in GEOS-Chem and shown to be negligible for locations very far from emission sources but in the range of ~1.5−8 ppm over large urban areas (Los Angeles, New York City, Berlin, Tehran, and Beijing). These numbers should be contrasted with the accuracy (~0.1 ppm) and precision (~0.2 ppm) of flask [*Conway et al.*, 1994] and continuous in situ [*Worthy et al.*, 2003] CO_2 measurements. Impacts of the combined temporal scaling on XCO_2 were found to reach as high as 0.1−0.5 ppm over the same major urban areas, with a larger proportion resulting from the weekly variability than with surface CO_2, which will be relevant for the assimilation of XCO_2 satellite observations.

[39] We also derive scale factors to account for the large per capita differences in CO_2 emissions between Canadian provinces. The NIR reported high per capita emissions for Alberta (13.68 Mg C person^{-1} yr^{-1}), related to the dependence on coal for electricity generation as well as the fossil fuel extraction and refining industries, and for Saskatchewan (11.94 Mg C person^{-1} yr^{-1}), for the same reasons, along with high off-road mobile emissions, presumably from farming. Low per capita emissions are found for some other provinces, including Quebec (2.19 Mg C person^{-1} yr^{-1}) and Manitoba (2.57 Mg C person^{-1} yr^{-1}), because of the high proportion of hydroelectric generation, and Ontario (2.92 Mg C person^{-1} yr^{-1}), because of the high proportion of non-CO_2-emitting electricity generation methods including nuclear, hydroelectric, and renewable energy, although differences in per capita total energy use are also a factor. Quantification of the impacts of these spatial scale factors for Canada will be investigated in future work.

[40] The resulting products of this work are a set of 24 diurnal and seven weekly global $0.25° \times 0.25°$ gridded temporal scale factor maps that can be applied to common global fossil fuel CO_2 emission inventories to represent weekly and diurnal variability and a set of $1° \times 1°$ spatial scale factor maps to adjust CDIAC and ODIAC to account for variability in per capita emissions within Canada. Both sets of scale factors (along with an additional set of weekly factors with no scaling for China and its proxy countries, based on the NO_2 analysis of *Beirle et al.* [2003]) are publicly available from CDIAC website. Implementation of

these temporal and spatial scale factors should contribute to a reduction in systematic errors related to CO_2 emissions from fossil fuel combustion and cement manufacture in the current generation of inverse modeling and data assimilation systems, which typically impose fossil fuel emissions and optimize fluxes from the terrestrial biosphere and oceans using atmospheric CO_2 point measurements. Scale factors such as these will be crucial for the more sophisticated systems being developed for assimilation of satellite CO_2 observations, intended for estimation of terrestrial and ocean fluxes at higher spatial and temporal scales. Future systems could also be used for deriving optimized estimates of CO_2 from fossil fuel emissions, in which these scale factors could be applied to yield improved temporal and spatial distributions in a priori estimates, which should lead to more accurate CO_2 emission quantification.

[41] **Acknowledgments.** R.N. thanks Michael Moran for helpful comments on an earlier version of the manuscript. R.J.A. was sponsored by the U.S. Department of Energy, Office of Science, Biological and Environmental Research (BER) programs, and work was performed at Oak Ridge National Laboratory (ORNL) under U.S. Department of Energy contract DE-AC05-00OR22725.

References

Andres, R. J., G. Marland, I. Fung, and E. Matthews (1996), A 1° × 1° distribution of carbon dioxide emissions from fossil fuel consumption and cement manufacture, 1950 – 1990, *Global Biogeochem. Cycles*, *10*(3), 419–429.

Andres, R. J., J. S. Gregg, L. Losey, G. Marland, and T. A. Boden (2011), Monthly, global emissions of carbon dioxide from fossil fuel consumption, *Tellus B*, *63B*, 309–327.

Andres, R. J., et al. (2012), A synthesis of carbon dioxide emissions from fossil fuel combustion, *Biogeosciences*, *9*, 1845–1871, doi:10.5194/bg-9-1845-2012.

Baker, D. F., et al. (2006), TransCom 3 inversion intercomparison: Impact of transport model errors on the interannual variability of regional CO_2 fluxes, 1988–2003, *Global Biogeochem. Cycles*, *20*, GB1002, doi:10.1029/2004GB002439.

Beirle, S., U. Platt, M. Wenig, and T. Wagner (2003), Weekly cycle of NO_2 by GOME measurements: a signature of anthropogenic sources, *Atmos. Chem. Phys.*, *3*, 2225–2232.

Boersma, K. F., D. J. Jacob, M. Trainic, Y. Rudich, I. DeSmedt, R. Dirksen, and H. J. Eskes (2009), Validation of urban NO_2 concentrations and their diurnal and seasonal variations observed from the SCIAMACHY and OMI sensors using in situ surface measurements in Israeli cities, *Atmos. Chem. Phys.*, *9*, 3867–3879.

Bovensmann, H., M. Buchwitz, J. P. Burrows, M. Reuter, T. Krings, K. Gerilowski, O. Schneising, J. Heymann, A. Tretner, and J. Erzinger (2010), A remote sensing technique for global monitoring of power plant CO_2 emissions from space and related applications, *Atmos. Meas. Tech.*, *3*, 781–811, 2010, doi:10.5194/amt-3-781-2010.

Buchwitz, M., O. Schneising, J. P. Burrows, H. Bovensmann, M. Reuter, and J. Notholt (2007), First direct observation of the atmospheric CO_2 year-to-year increase from space, *Atmos. Chem. Phys.*, *7*, 4249–4256.

Conway, T. J., P. P. Tans, L. S. Waterman, K. W. Thoning, D. R. Kitzis, K. A. Masarie, and N. Zhang (1994), Evidence for interannual variability of the carbon cycle from the National Oceanic and Atmospheric Administration/Climate Monitoring and Diagnostics Laboratory Global Air Sampling Network, *J. Geophys. Res.*, *99*(D11), 22831–22855.

Corbin, K., S. Denning, and K. R. Gurney (2010), Effects of spatially and temporally redistributing fossil fuel emissions on atmospheric CO_2 concentrations, *Tellus*, *62B*, 506–511, doi:10.1111/j.1600-0889.2010.00480.x

Coutts, A. M., J. Beringer, and N. J Tapper (2007), Characteristics influencing the variability of urban CO_2 fluxes in Melbourne, Australia, *Atmos. Environ.*, *41*, 51–62.

Crisp, D., et al. (2004), The Orbiting Carbon Observatory (OCO) mission, *Adv. Space Res.*, *34*, 700–709.

Crisp, D., et al. (2012), The ACOS CO_2 retrieval algorithm—Part II: Global X_{CO2} data characterization, *Atmos. Meas. Tech.*, *5*, 687–707, 2012, doi:10.5194/amt-5-687-2012.

Erickson, D. J., III, R. T. Mills, J. Gregg, T. J. Blasing, F. M. Hoffman, R. J. Andres, M. Devries, Z. Zhu, and S. R. Kawa (2008), An estimate of monthly global emissions of anthropogenic CO_2: Impact on the seasonal cycle of atmospheric CO_2, *J. Geophys. Res.*, *113*, G01023, doi:10.1029/2007JG000435.

Gavison, R., and N. Perez (2007), Days of rest in multicultural societies: Private, public, separate? (June 11, 2007). Constituting Religion: Law, Society and Faith in the 21st Century, edited by P. Cane, C. Evans, and Z. Robinson. Available at SSRN: http://ssrn.com/abstract=1862906.

Guan, D., Z. Liu, Y. Geng, S. Lindner, and K. Hubacek (2012), The gigatonne gap in China's carbon dioxide inventories, *Nat. Clim. Change*, *2*, 672–675, doi:10.1038/nclimate1560.

Gurney, K. R., et al. (2002), Towards robust regional estimates of CO_2 sources and sinks using atmospheric transport models, *Nature*, *415*, 626–630.

Gurney, K. R., et al. (2004), Transcom 3 inversion intercomparisons: Model mean results for the estimation of seasonal carbon sources and sinks, *Global Biogeochem. Cycles*, *18*, GB1010, doi:10.1029/2003GB002111.

Gurney, K. R., Y.-H. Chen, R. Maki, S. R. Kawa, A. Andrews, and Z. Zhu (2005), Sensitivity of atmospheric CO_2 inversions to seasonal and interannual variations in fossil fuel emissions, *J. Geophys. Res.*, *10*, D10308.

Gurney, K. R., et al. (2009), High resolution fossil fuel combustion CO_2 emission fluxes for the United States, *Environ. Sci. Technol.*, *43*, 5535–5541.

Hoornweg, D., L. Sugar, and C. L. T. Gomez (2011), Cities and greenhouse gas emissions: moving forward, *Environ. Urbanization*, *23*, 207–227, doi:10.1177/0956247810392270.

Kühlwein, J., B. Wickert, A. Trunkmüller, J. Theloke, and R. Friedrich (2002), Emission modelling in high spatial and temporal resolution and calculation of pollutant concentrations for comparisons with measured concentrations, *Atmos. Environ.*, *36*, 7–18, doi:10.1016/s1352-2310(02)00209-1.

Levin, I., S. Hammer, E. Eichelmann, and F. R. Vogel (2011), Verification of greenhouse gas emission reductions: the prospect of atmospheric monitoring in polluted areas, *Phil. Trans. R. Soc. A.*, *369*, 1906–1924, doi:10.1098/rsta.2010.0249.

Maksyutov, S., *et al*. (2012), Regional CO_2 flux estimates for 2009-2010 based on GOSAT and ground-based CO_2 observations, *Atmos. Chem. Phys. Discuss.*, *12*, 29235–29288, doi:10.5194/acpd-12-29235-2012.

McKain, K., S. C. Wofsy, T. Nehrkorn, J. Eluszkiewicz, J. Ehleringer, and B. Stephens (2012), Assessment of ground-based atmospheric observations for verification of greenhouse gas emissions from an urban region, *Proc. Natl. Acad. Sci. U.S.A.*, *109*(22), 8423–8428.

Miller, J. B., et al. (2012), Linking emissions of fossil fuel CO_2 and other anthropogenic trace gases using atmospheric $^{14}CO_2$, *J. Geophys. Res.*, *117*, D08302, doi:10.1029/2011JD017048.

Nassar, R., et al. (2010), Modeling global atmospheric CO_2 with improved emission inventories and CO_2 production from the oxidation of other carbon species, *Geosci. Model Dev.*, *3*, 689–716.

Nassar, R., et al. (2011), Inverse modeling of CO_2 sources and sinks using satellite observations of CO_2 from TES and surface flask measurements, *Atmos. Chem. Phys.*, *11*, 6029–6047.

National Inventory Report 1990–2009: Greenhouse Gas Sources and Sinks in Canada (2011), ISSN: 1706-3353, Cat. No.: En81-4/2009E-PDF.

Oda, T., and S. Maksyutov (2011), A very high-resolution (1 km × 1 km) global fossil fuel CO_2 emission inventory derived using a point source database and satellite observations of nighttime lights, *Atmos. Chem. Phys.*, *11*, 543–556, doi:10.5194/acp-11-543-2011.

Olsen, S. C., and J. T. Randerson (2004), Differences between surface and column atmospheric CO_2 and implications for carbon cycle research, *J. Geophys. Res.*, *109*, D02301, doi:10.1029/2003JD003968.

Pacala, S., et al. (2010), Verifying greenhouse gas emissions: methods to support international climate agreements. Committee on Methods for Estimating Greenhouse Gas Emissions, National Research Council Report, National Academies Press, Washington, D. C., ISBN 978-0-309-15211-2.

Peters, G. P., G. Marland, C. LeQuere, T. Boden, J. G. Candell, and M. R. Raupach (2011), Rapid growth in CO_2 emissions after the 2008 – 2009 global financial crisis, *Nat. Clim. Change*, *2*, 2–4.

Peters, W., et al. (2005), An atmospheric perspective on North American carbon dioxide exchange: CarbonTracker, *Proc. Natl. Acad. Sci. U.S.A.*, *104*(48), 18925–18930, doi:10.1073/pnas.0708986104/PNAS, 2007.

Peters, W., et al. (2007), Seven years of recent European net terrestrial carbon dioxide exchange constrained by atmospheric observations, *Global Change Biol.*, *16*(4), 1317–1337.

Pétron, G., P. Tans, G. Frost, D. Chao, and M. Trainer (2008), High resolution emission of CO_2 from power plants in the USA, *J. Geophys. Res.*, *113*, G04008, doi:10.1029/2007JG000602.

Peylin, P., et al. (2011), Importance of fossil fuel emission uncertainties over Europe for CO_2 modeling: Model intercomparison, *Atmos. Chem. Phys.*, *11*, 6607–6622, 2011, doi:10.5194/acp-11-6607-2011.

Pregger, T., Y. Scholz, and R. Friedrich (2007), Documentation of the anthropogenic GHG emission data for Europe provided in the frame of CarboEurope GHG and CarboEurope IP, Institute of Energy Economics and the Rational Use of Energy (IER), University of Stuttgart.

Rayner, P. J., M. R. Raupach, M. Paget, P. Peylin, and E. Koffi (2010), A new global gridded data set of CO_2 emissions from fossil fuel combustion: Methodology and evaluation, *J. Geophys. Res.*, *115*, D19306, doi:10.1029/2009JD013439.

Schuh, A. E., A. S. Denning, K. D. Corbin, I. T. Baker, M. Uliasz, N. Parazoo, A. E. Andrews, and D. E. J. Worthy (2010), A regional high-resolution carbon flux inversion for North America for 2004, *Biogeosciences*, *7*, 1625−1644, doi:10.5194/bg-7-1625-2010.

Steinbach, J., C. Gerbig, C. Rödenbeck, U. Karstens, C. Minejima, and H. Mukai (2011), The CO_2 Release and Oxygen Uptake from Fossil Fuel Emission Estimate (COFFEE) data set: Effects from varying oxidative ratios, *Atmos. Chem. Phys.*, *11*, 6855−6870, doi:10.5194/acp-11-6855/2011/.

Takagi, H., et al. (2011), On the benefit of GOSAT observations to the estimation of regional CO_2 fluxes, *Sci. Online Lett. Atmos.*, *7*, 161−164, doi:10.2151/sola.2011-041.

Turnbull, J., P. Rayner, J. Miller, T. Naegler, P. Ciais, and C. Cozic (2009), On the use of $^{14}CO_2$ as a tracer for fossil fuel CO_2: Quantifying uncertainties using an atmospheric transport model, *J. Geophys. Res.*, *114*, D22302, doi:10.1029/2009JD012308.

Vogel, F. R., S. Hammer, A. Steinhof, B. Kromer, and I. Levin (2010), Implication of weekly and diurnal ^{14}C calibration on hourly estimates of CO-based fossil fuel CO_2 at a moderately polluted site in southwestern Germany, *Tellus*, *62B*, 512–520, doi:10.1111/j.1600-0889.2010.00477.x.

Vogt, R., A. Christen, M. W. Rotach, M. Roth, and A. N. V. Satyanarayana (2005), Temporal dynamics of CO_2 fluxes and profiles over a Central European city, *Theor. Appl. Climatol.*, *84*, 117−126, DOI: 10.1007/s00704-005-0149-9.

Worthy, D. E. J., K. Higuchi, and D. Chan (2003), North American influence on atmospheric carbon dioxide data collected at Sable Island, Canada, *Tellus 55B*, 105−114.

Wunch, D., G. C. Toon, J.-F. L. Blavier, R. A. Washenfelder, J. Noholt, B. J. Connor, D. W. T Griffith, V. Sherlock, and P. O. Wennberg (2011), The Total Carbon Column Observing Network, *Philos. Trans. R. Soc. A*, *369*, 2087−2112, doi:10.1098/rsta.2010.0240.

Yokota, T., Y. Yoshida, N. Eguchi, Y. Ota, T. Tanaka, H. Watanabe, and S. Maksyutov (2009), Global concentrations of CO_2 and CH_4 Retreived from GOSAT: First Preliminary Results, *Sci. Online Lett. Atmos.*, *5*, 160–163, doi:10.2151/sola.2009-041.

Yoshida, Y., Y. Ota, N. Eguchi, N. Kikuchi, K. Nobuta, H. Tran, I. Morino, and T. Yokota (2011), Retrieval algorithm for CO_2 and CH_4 column abundances from short-wavelength infrared spectral observations by the Greenhouse Gases Observing Satellite, *Atmos. Meas. Tech.*, *4*, 717–734, doi:10.5194/amt-4-717-2011.

Zhou, Y., and K. R. Gurney (2011), Spatial relationships of sector-specific fossil fuel CO_2 emissions in the United States, *Global Biogeochem. Cycles*, *25*, GB3002, doi:10.1029/2010GB00382.